American Journal of Advanced Materials Research (AJAMR)

ISSN: 3070-2011 (ONLINE)

VOLUME 2 ISSUE 1 (2026)

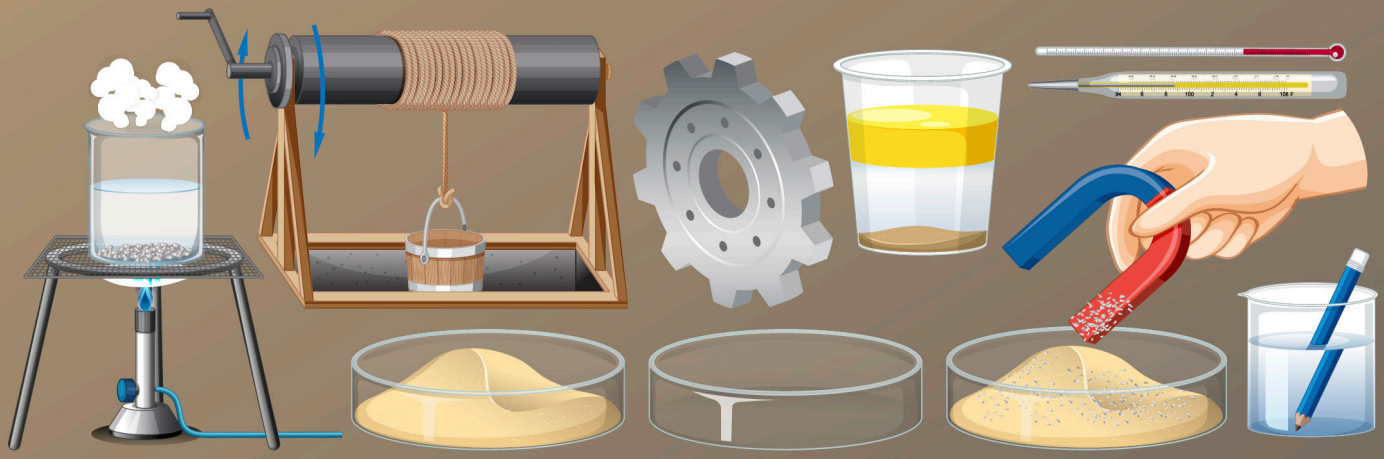

PUBLISHED BY
E-PALLI PUBLISHERS, DELAWARE, USA

American Journal of
Advanced Materials Research (AJAMR)

Volume 2 Issue 1, Year 2026
ISSN: 2158-8155 (Online), 2832-4854 (Print)
DOI: https://doi.org/10.54536/ajamr.v2i1.7397
https://journals.e-palli.com/home/index.php/ajamr

Nonlinear Model for Cancer Dynamics

Matheus dos Santos Farias[1*]

Article Information

Received: January 20, 2026

Accepted: April 04, 2026

Published: June 06, 2026

Keywords

Chaos Theory, Delay Differential Equations, Dynamical Systems, Nonlinear Model, Tumor

ABSTRACT

This study proposes a nonlinear model for cancer dynamics over a 12-month period, using delay differential equations (DDEs) inspired by the Lorenz system. The modeling focuses solely on the internal evolution of the tumor, excluding any interaction with the immune system or clinical treatments, and emphasizes cellular proliferation, mutation, and angiogenesis. The model progressively incorporates the delay parameter τ, which represents biological memory effects, allowing for the analysis of dynamic transitions in the system from stability to chaotic behavior. The approach employs tools from chaos theory, bifurcation analysis, and dynamic systems, with tumor behavior graphically represented through phase portraits ($z(t)\times y(t)$). Numerical simulations were carried out using the fourth-order Runge-Kutta method, implemented in Python, and supported by the NumPy, SciPy, and Matplotlib libraries. The results show that cancer can evolve from a stable state to highly disordered dynamics as time progresses and memory effects intensify, reflecting patterns observed in aggressive tumors. This model contributes to a deeper understanding of the complexity of tumor growth and may serve as a foundation for future predictive strategies in precision medicine.

INTRODUCTION

Cancer

Cancer is a disease characterized by the uncontrolled proliferation of abnormal cells in the body, which can invade adjacent tissues and, in many cases, metastasize to distant organs. This process results from genetic mutations that disrupt the regulation of the cell cycle and apoptosis. The term cancer dates back to antiquity, but it was the Greek physician Hippocrates (c. 460–370 BC) who first used the terms carcinoma and carcinos to describe tumors, inspired by their resemblance to crab legs. Today, cancer remains one of the leading causes of mortality worldwide, particularly in forms such as lung, breast, prostate, and colorectal cancers (Ferlay *et al.* 2020). According to Bray *et al.* (Bray *et al.* 2018), understanding the dynamics of cancer growth is essential for developing effective strategies for treatment, control, and prevention.

Immune System

The immune system is responsible for protecting the body against pathogens such as viruses, bacteria, and abnormal cells, including tumor cells. It consists of specialized cells such as T lymphocytes, B lymphocytes, macrophages, and natural killer (NK) cells that participate in both innate and adaptive immune responses. Under normal physiological conditions, the immune system is capable of recognizing and eliminating potentially cancerous cells. However, tumors often develop immune evasion mechanisms, which hinder their detection and destruction (Binnewies *et al.* 2018). Understanding the complex interactions between the immune system and cancer is fundamental to the development of modern immunotherapies, including immune checkpoint inhibitors (Chen and Mellman 2017).

For this study, it was decided not to consider the immune system, medical treatments or other external interventions. The focus is exclusively on the internal dynamics of tumor growth, which allows simplifying the mathematical modeling and clearly analyzing the mechanisms that lead to the transformation of a benign tumor into malignant cancer.

Motivation

The motivation for this study lies in the need to better understand the dynamics of tumor growth through mathematical modeling. As noted by Cardoso (Cardoso 2021), mathematical models are valuable tools for predicting cancer behavior, enabling the simulation of tumor evolution over time. Furthermore, Reis and Almeida (Reis and Almeida 2020) emphasize that such approaches contribute to the analysis of mechanisms underlying the transformation of a tumor into malignant cancer, thereby supporting advances in biomedical research. In this work, we chose to isolate the internal dynamics of tumor development, deliberately excluding external factors such as treatments, immune responses, or clinical interventions. This simplification facilitates the construction of the model and allows for a clearer analysis of intrinsic cell growth patterns.

Theoretical Framework

The objective of this chapter is to present the theoretical foundations that support this work. It begins with a discussion of dynamical systems, highlighting key concepts such as phase space, equilibrium points, stability, linear stability, bifurcations, and chaos. The chapter concludes with an overview of the numerical methods

[1] Hospital Albert Einstein, São Paulo, Brazil
[*] Corresponding author's e-mail: matheusfariasfm@gmail.com

used and considerations regarding delay differential equations.

Dynamic Systems

Dynamical systems constitute a branch of applied mathematics and physics that studies the temporal evolution of variables within a given state space. These systems are formally described by equations that determine how the state of a system changes over time, and are generally categorized into two main types: discrete and continuous (Strogatz 2018).

Discrete Dynamical Systems

In these systems, variables evolve at discrete time steps and are often modeled by function iterations. A classical example is the discrete-time Lotka–Volterra predator-prey system:

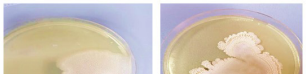

1 y_n population and y_n the predator population at time n. Another relevant example is the logistic model with limited growth:

$$x_{n+1} = x_n\left(1 + r\left(1 - \frac{x_n}{K}\right)\right),$$

d K is the carrying capacity of the environment.

Continuous Dynamical Systems

They are described by ordinary differential equations (ODEs), representing continuous changes in time. The general form is:

dx/dt=f(x,t),

with x(t)∈R^n and f:R^n×R→R^n a sufficiently regular function. These systems allow the study of stability, bifurcations and chaotic behavior in biological contexts, such as the evolution of cancer (Perko, 2013).

State Space or Phase Space

The state space, also known as phase space, is a multidimensional space that represents the evolution of a dynamical system. Each point in this space corresponds to a complete state of the system, defined by its dynamical variables at a given time.

The system's behavior over time is described by a set of ordinary differential equations:

$$\frac{d\boldsymbol{x}}{dt} = \boldsymbol{f}(\boldsymbol{x},t), \quad \boldsymbol{x} = \begin{bmatrix} x_1 \\ x_2 \\ \vdots \\ x_n \end{bmatrix}, \quad \boldsymbol{f}(\boldsymbol{x},t) = \begin{bmatrix} f_1(\boldsymbol{x},t) \\ f_2(\boldsymbol{x},t) \\ \vdots \\ f_n(\boldsymbol{x},t) \end{bmatrix}$$

ns can be done by the Jacobian matrix J, defined as the matrix of partial derivatives of the vector function f:

$$\boldsymbol{J}(\boldsymbol{x}) = \begin{bmatrix} \frac{\partial f_1}{\partial x_1} & \frac{\partial f_1}{\partial x_2} & \cdots & \frac{\partial f_1}{\partial x_n} \\ \frac{\partial f_2}{\partial x_1} & \frac{\partial f_2}{\partial x_2} & \cdots & \frac{\partial f_2}{\partial x_n} \\ \vdots & \vdots & \ddots & \vdots \\ \frac{\partial f_n}{\partial x_1} & \frac{\partial f_n}{\partial x_2} & \cdots & \frac{\partial f_n}{\partial x_n} \end{bmatrix}$$

n points is determined by the eigenvalues λ of the Jacobian, obtained by solving the characteristic equation:

det(J-λI)=0

If all eigenvalues have a negative real part, the equilibrium point is asymptotically stable; otherwise, it may be unstable or a saddle point (Khalil, 2018).

Equilibrium and Stability Points

The equilibrium points of a dynamic system are the states in which the variables do not change over time, that is, the rate of change of the state variables is zero. For an autonomous system of the form

dx/dt=f(x),

an equilibrium point x* satisfies the condition

f(x*)=0.

The local stability of x* can be investigated by means of the derivative of f, that is, by the Jacobian matrix evaluated at x*:

J=∂f/∂x $|_{x=x^*}$.

Consider the two-dimensional linear system:

(dx/dt&=ax+by,dy/dt&=cx+dy.)

The Jacobian matrix of this system is given by:

$$J = \begin{bmatrix} \frac{\partial f_1}{\partial x} & \frac{\partial f_1}{\partial y} \\ \frac{\partial f_2}{\partial x} & \frac{\partial f_2}{\partial y} \end{bmatrix} = \begin{bmatrix} a & b \\ c & d \end{bmatrix}.$$

are found by solving the characteristic polynomial:

det(J-λI)=0,

that is,

According to the Linear Stability Theorem (Strogatz,

$$\Delta X = \epsilon \cdot X_n + \delta_1 \cdot \nabla X.$$

2018), if all eigenvalues of J have a negative real part, the equilibrium point x* is asymptotically stable. If at least one eigenvalue has a positive real part, the point is unstable.

Linear Stability

The linear stability of a dynamical system can be analyzed in the vicinity of an equilibrium point through linearization. Consider a two-dimensional system described by the differential equations:

(dx/dt&=f(x,y),dy/dt&=g(x,y),)

The Jacobian matrix associated with the system, evaluated at an equilibrium point (x*,y*), is given by:

To determine the eigenvalues λ of the linearized system,

$$J = \begin{bmatrix} \frac{\partial f}{\partial x} & \frac{\partial f}{\partial y} \\ \frac{\partial g}{\partial x} & \frac{\partial g}{\partial y} \end{bmatrix}|_{(x^*,y^*)}.$$

solve the characteristic equation:
det(J-λI)=0,
I.e,
The nature of the eigenvalues obtained — in particular,

$$\det\begin{bmatrix} \frac{\partial f}{\partial x} - \lambda & \frac{\partial f}{\partial y} \\ \frac{\partial g}{\partial x} & \frac{\partial g}{\partial y} - \lambda \end{bmatrix} = \left(\frac{\partial f}{\partial x} - \lambda\right)\left(\frac{\partial g}{\partial y} - \lambda\right) - \frac{\partial f}{\partial y}\frac{\partial g}{\partial x} = 0.$$

the sign of their real parts — determines the stability of the equilibrium point, according to the Linear Stability Theorem.
As an example, consider the following nonlinear system:
(dx/dt&=x(1-x)-y/K, dy/dt&=α/(1+x)-βy,)
where K, α and β are positive parameters. The corresponding Jacobian matrix is:
The characteristic equation is therefore:

$$J = \begin{bmatrix} 1 - 2x & -\frac{1}{K} \\ -\frac{\alpha}{(1+x)^2} & -\beta \end{bmatrix}|_{(x^*,y^*)}.$$

(1-2x*-λ)(-β-λ)+α/(K(1+x*)^2)=0.
The analysis of the roots of this equation allows us to determine the local stability of the equilibrium point (x*,y*).

Classification of Equilibrium Points
The classification of equilibrium points is based on the eigenvalues obtained from the linearized Jacobian matrix. Depending on the signs of the real parts of these eigenvalues, the equilibrium points can be classified as follows:

Stable Equilibrium Point (attractor)
If both eigenvalues have negative real parts, the equilibrium point is stable; that is, the system's solutions return to the equilibrium point after small perturbations.

Unstable Equilibrium Point (repeller)
If both eigenvalues have positive real parts, the equilibrium point is unstable, and the system's solutions diverge from the equilibrium.

Saddle Point
If the eigenvalues have real parts with opposite signs, the equilibrium point is a saddle point, exhibiting direction-dependent stability—stable in one direction and unstable in another.
Considering the eigenvalues λ_1 and λ_2, the classification can be summarized as follows:
"Stable point:" "Re"(λ_1)<0, "Re"(λ_2)<0
"Unstable point:" "Re"(λ_1)>0, "Re"(λ_2)>0
"Saddle point:" "Re"(λ_1)·"Re"(λ_2)<0
Where "Re"(λ) denotes the real part of the eigenvalue λ.
Linearization and Nonlinear Stability
Linearization of a nonlinear system around an equilibrium point is a valuable technique for analyzing the local stability of dynamical systems. However, this method may not accurately capture the system's behavior in regions far from the equilibrium, where nonlinear effects dominate and more complex dynamics may arise. For a general nonlinear system described by the equations:
(dx/dt&=f(x), dy/dt&=g(y),)
where f(x) and g(y) are non-linear functions, linearization consists of approximating the behavior of the system through an expansion around the equilibrium point, (x*,y*), as:
Δx=x-x*, Δy=y-y*, Δx Δx=f(x*)+J·Δx, Δy ̇=g(y^*)+J·Δy.
Where J is the Jacobian matrix, and the terms f(x^*) and g(y*) are the evaluations of the dynamics function at the equilibrium point. The analysis of nonlinear stability requires additional techniques, such as the study of bifurcations and limit cycles.

Limit Cycles
Limit cycles are periodic solutions of a dynamical system that arise in nonlinear regimes, typically through bifurcation phenomena. They represent stable or unstable closed trajectories in phase space, to which nearby trajectories may converge or diverge over time.A common mechanism for the emergence of limit cycles is the Hopf bifurcation, in which an equilibrium point loses stability and gives rise to a stable periodic orbit. An illustrative second-order linear differential equation that may exhibit oscillatory behavior under certain parameter conditions is given by:
(d^2 x)/(dt^2)+α dx/dt+βx=0,
where α and β are constants. Although this equation alone does not generate limit cycles (being linear), its nonlinear extensions can lead to self-sustained oscillations. When the parameters reach a critical value, the system may begin to oscillate periodically, potentially forming a limit cycle in a corresponding nonlinear formulation. In addition, a limit cycle is often associated with a bifurcation, where an equilibrium point loses its stability and transforms into a stable or unstable cycle, as the system parameter is adjusted. The general equation for the occurrence of a limit cycle in nonlinear systems with delay is:
dx/dt=λx-μx^3+γ (dx(t-τ))/dt,
where τ is the delay time, and λ, μ, and γ are parameters that determine the amplitude and frequency of the limit cycle.

Bifurcations
Bifurcations are phenomena where a small variation in the system parameters can result in a qualitative change in its behavior. Some common types of bifurcations in dynamical systems are presented below.

Tangent (Saddle-Node or Bend) Bifurcation
A saddle-node or bend bifurcation occurs when two equilibrium points approach each other, merge, and then annihilate each other as the control parameter is changed. The system is given by:

$dx/dt=\mu x-x^3$

The Jacobian associated with the equilibrium point x* is given by:

$J=d/dx(\mu x-x^3)=\mu-3x^2$.

When μ=0, the equilibrium points merge, resulting in a qualitative change in the system.

The graph above represents the saddle-node bifurcation (or bending) associated with the equation:

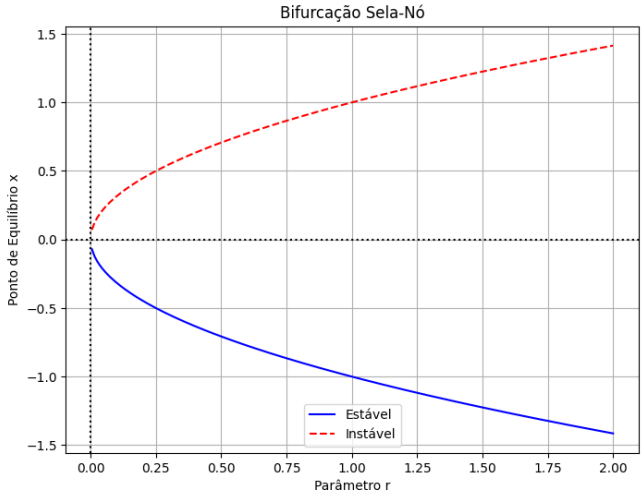

Figure 1: Bifurcation diagram of [eq:saddle_node] showing the saddle-node bifurcation

$dx/dt=r+x^2$

The dynamics of the system vary according to the parameter r:

• For r<0: there is no real equilibrium point, since the equation $r+x^2=0$ has no real solution.

• For r=0: bifurcation occurs. Two equilibrium points collide and cancel each other out at the critical point.

• For r>0: two real equilibrium points appear:

$x=-\sqrt{r}$: stable equilibrium point (represented by the solid blue curve).

$x=+\sqrt{r}$: unstable equilibrium point (represented by the dashed red curve).

This phenomenon is characteristic of saddle-node bifurcation, where pairs of equilibria are created or destroyed as the parameter is adjusted.

Transcritical Bifurcation

In transcritical bifurcation, two equilibrium points exchange stability. As the control parameter varies, the roots of the system cross.

The system is given by:

$$\begin{equation} \frac{dx}{dt} = \mu x - x^2 + \beta y\label{eq:transcritical}\end{equation}$$

The Jacobian associated with the equilibrium point (x*,y*) is:

Transcritical bifurcation occurs when two equilibrium points exchange stability as the control parameter varies.

$$F(t,u) = \frac{1}{h}\int_t^{t+h} f\left(\zeta, u(\zeta)\right) d\zeta$$

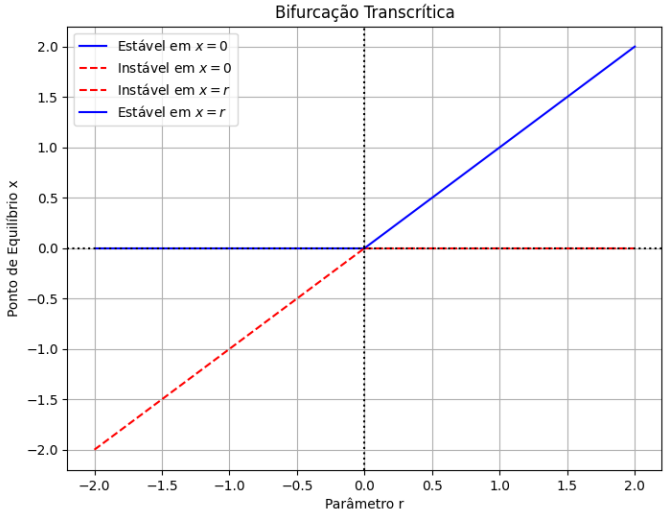

Figure 2: Bifurcation diagram of [eq:transcritical] showing the transcritical bifurcation

The equation that models this type of bifurcation is $dx/dt=rx-x^2$, in which the equilibrium points are given by x=0 and x=r. For values of r<0, the point x=0 is stable, while the point x=r is unstable. When r>0, a switch occurs: x=0

becomes unstable and x=r becomes stable. This switch in stability at the critical point r=0 characterizes transcritical bifurcation, in which the equilibria cross and switch between stable and unstable nature.

The behavior of the roots and the switch in stability depend on the value of the parameter μ, leading to the switch in stability between the equilibrium points.

Pitchfork Cusp

A pitchfork bifurcation occurs when a stable equilibrium point splits into three equilibrium points. This bifurcation is characterized by the formation of one unstable equilibrium point and two stable equilibrium points. The system is given by:

$dx/dt=\mu x-x^3$,

The Jacobian associated with the equilibrium point x* is:

$J=d/dx(\mu x-x^3)=\mu-3x^2$.

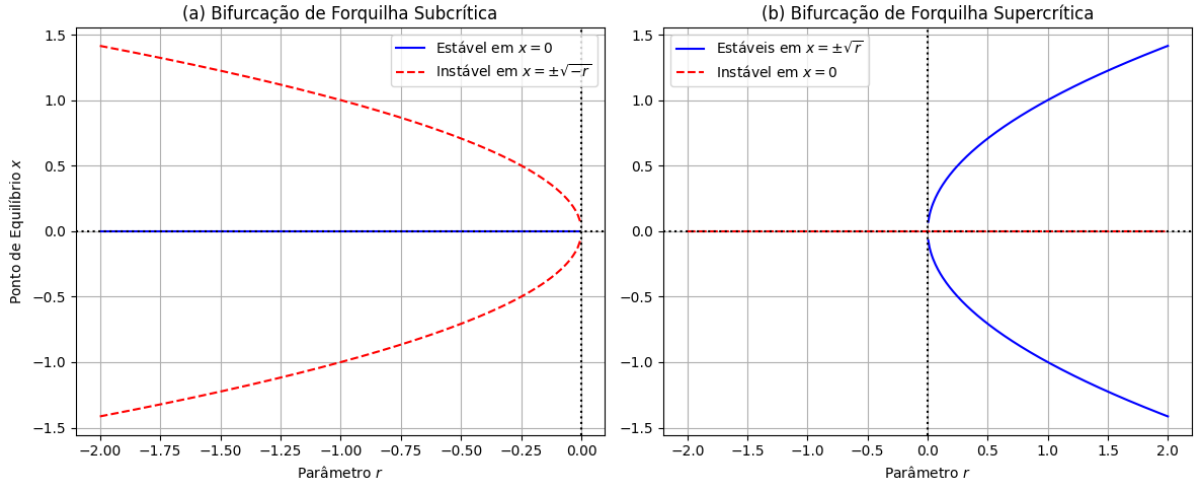

Figure 3: Bifurcation diagram showing subcritical fork in (a) and supercritical bifurcation in (b)

When μ is negative, the equilibrium point is unique and stable. When μ becomes positive, the equilibrium point splits into three.

Hopf Bifurcation

A Hopf bifurcation occurs when a stable equilibrium point becomes unstable, and a limit cycle begins to form. This generates oscillations in the system, which characterizes the Hopf bifurcation.

The system is given by:

$dx/dt=\mu x-y-x^3$,

$dy/dt=x+\mu y$.

The Jacobian associated with the equilibrium point (x*,y*) is:

When the parameter μ is changed, the equilibrium point starts to have a limit cycle around itself, indicating the transition to oscillatory behavior in the system.

$$J=\begin{pmatrix}\frac{\partial f}{\partial x} & \frac{\partial f}{\partial y}\\ \frac{\partial g}{\partial x} & \frac{\partial g}{\partial y}\end{pmatrix}_{(x^*,y^*)}=\begin{pmatrix}\mu-3(x^*)^2 & -1\\ 1 & \mu\end{pmatrix}.$$

The Figure [fig:hopf-diagram] shows the supercritical and subcritical Hopf bifurcation diagrams. In the supercritical

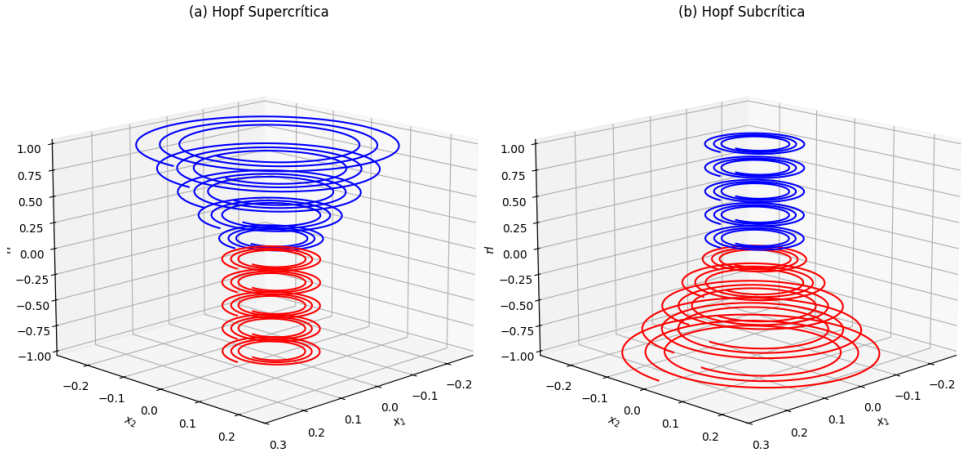

Figure 4: Bifurcation diagrams showing the Hopf bifurcation (a) Supercritical and (b) Subcritical

case, as the bifurcation parameter μ exceeds zero, the equilibrium point loses stability and a stable limit cycle with increasing radius (blue spiral) emerges. In the subcritical case, an unstable limit cycle (in red) exists for $\mu<0$ and collapses into the unstable equilibrium point as $\mu\to0^-$, characterizing a qualitatively distinct behavior

between the two bifurcations.

Chaos

Chaos, in the context of dynamical systems, refers to an apparently random and unpredictable behavior that emerges from nonlinear deterministic systems. Although these systems follow well-defined equations, small variations in the initial conditions can generate significantly different trajectories over time, a phenomenon known as sensitivity to initial conditions. From a mathematical point of view, a chaotic system is deterministic (i.e., without stochastic components), but exhibits highly sensitive and complex behavior, which makes it practically unpredictable in the long term. Three fundamental characteristics are present in chaotic systems:

- Sensitivity to initial conditions;
- Topological intransitivity;
- Density of periodic orbits.

A rigorous mathematical definition of chaos has been proposed based on the Lyapunov exponents, which quantify the degree of exponential separation between initially close trajectories. Let λ be a Lyapunov exponent; if the largest exponent $\lambda_{max} > 0$, the system is considered chaotic. Formally:

where δ(0) is an infinitesimal initial perturbation and δ(t) represents the separation between trajectories at time t.

$$\lim_{t\to\infty} \frac{1}{t} \ln\left(\frac{|\delta(t)|}{|\delta(0)|}\right) = \lambda,$$

An example of a modified chaotic dynamical system can be given by the following nonlinear differential equations with harmonic perturbations and quadratic terms:

In this system, the parameters δi, ηi and k add extra nonlinearities that intensify the chaotic behavior.

$$\frac{dX}{dt} = \sigma(Y - X) + \delta_1 \cdot \sin(kX) + \eta_1 \cdot Z^2,$$
$$\frac{dY}{dt} = X(\rho - Z) - Y + \delta_2 \cdot \cos(kY) + \eta_2 \cdot XY,$$
$$\frac{dZ}{dt} = XY - \beta Z + \delta_3 \cdot \tan(kZ) + \eta_3 \cdot Y^2.$$

Considering initial perturbations in the variables:

where ϵ is a small positive constant, and ∇X, ∇Y, ∇Z represent local gradients.

$$\Delta X = \epsilon \cdot X_0 + \delta_1 \cdot \nabla X,$$
$$\Delta Y = \epsilon \cdot Y_0 + \delta_2 \cdot \nabla Y,$$
$$\Delta Z = \epsilon \cdot Z_0 + \delta_3 \cdot \nabla Z,$$

By substituting these perturbations into equations (1)–(3), it is found that even small variations in X_0, Y_0 and Z_0 result in completely distinct trajectories over time, evidencing the chaotic nature of the system. The analysis of these equations reveals that the nonlinear interactions between the variables, coupled with terms such as sin(kX), cos(kY) and tan(kZ), and the quadratic contributions (Z^2, XY, Y^2), are responsible for an extremely sensitive and unpredictable behavior. The positive value of the largest Lyapunov exponent in this context is what strictly characterizes chaos.

"Chaos is not random disorder, but complex order in a deterministic system."

The logistic map is given by:

$x_{n+1} = r x_n (1 - x_n)$

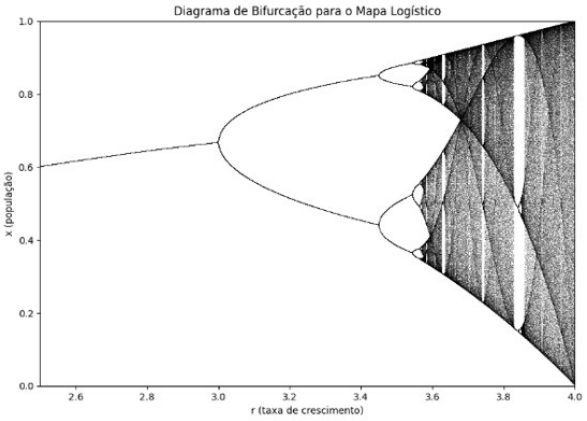

Figure 5: Bifurcation Diagram: Logistic Map

Where x_n is the population at iteration n, and r is the growth rate. The bifurcation diagram shows how the population fluctuates as r varies, revealing chaotic patterns when r is large.

MATERIALS AND METHODS

Methods in Dynamical Systems

The methods applied to dynamical systems aim to model the behavior of systems that evolve in time, especially those with multiple variables and complex interactions. An effective way to represent these interactions is through matrices and systems of vector differential equations. Consider a state vector X(t) that describes the temporal evolution of a system with variables x_i, y_j, z_k, influenced by constant coefficients a_{ij}, b_{ij}, c_{ij} and diffusion terms $\delta_i \cdot \nabla x_i$. The system can be represented in matrix form as follows:

$$\boldsymbol{X}(t) = \begin{pmatrix} \sum_{i=1}^{N} a_{1i}\, x_i + \sum_{j=1}^{M} b_{1j}\, y_j + \sum_{k=1}^{L} c_{1k}\, z_k + \delta_1 \cdot \nabla x_1 \\ \sum_{i=1}^{N} a_{2i}\, x_i + \sum_{j=1}^{M} b_{2j}\, y_j + \sum_{k=1}^{L} c_{2k}\, z_k + \delta_2 \cdot \nabla x_2 \\ \sum_{i=1}^{N} a_{3i}\, x_i + \sum_{j=1}^{M} b_{3j}\, y_j + \sum_{k=1}^{L} c_{3k}\, z_k + \delta_3 \cdot \nabla x_3 \\ \sum_{i=1}^{N} a_{4i}\, x_i + \sum_{j=1}^{M} b_{4j}\, y_j + \sum_{k=1}^{L} c_{4k}\, z_k + \delta_4 \cdot \nabla x_4 \\ \sum_{i=1}^{N} a_{5i}\, x_i + \sum_{j=1}^{M} b_{5j}\, y_j + \sum_{k=1}^{L} c_{5k}\, z_k + \delta_5 \cdot \nabla x_5 \\ \sum_{i=1}^{N} a_{6i}\, x_i + \sum_{j=1}^{M} b_{6j}\, y_j + \sum_{k=1}^{L} c_{6k}\, z_k + \delta_6 \cdot \nabla x_6 \end{pmatrix}$$

Numerical Methods

Numerical methods are techniques used to obtain approximations of solutions to mathematical problems that cannot be solved analytically. When a differential

equation does not have an exact solution or is difficult to obtain, numerical methods offer a way to efficiently approximate the solution.

For example, for an initial value problem (IVP), such as the system described by the differential equation:

$du/dt=f(t,u)$, $u(t_0)=u_0$,

A numerical method, such as the single-step method, can be used to estimate u(t) at future times from u_0. The exact solution of a differential equation can be expressed as an integral:

$$u(t+h) = u(t) + \int_t^{t+h} f(\zeta, u(\zeta))\, d\zeta.$$

However, this form is not directly usable due to the dependence of the solution u(ζ) on the integral. To solve this, the integral is approximated by numerical quadrature, resulting in a discrete form:

$$u(t+h) \approx u(t) + h \cdot f(t, u(t)).$$

This method provides an approximation of the solution at t+h from u(t), using information known at time t. Numerical methods are essential for solving complex problems in dynamical systems, bifurcations, and chaos, where the behavior of the system is highly sensitive to the initial conditions and parameters, making analytical solutions difficult.

Simple-Step Methods

Let us consider a system described by the ordinary differential equation presented in [eq:ivp], and suppose that t_0 represents the initial instant of time, with initial condition $u(t_0)=u_0$. According to Burden and Faires (2010), simple explicit methods consist of numerical strategies to estimate the value of the function u(t) at future instants from information known at the current instant. Such methods are especially useful when we seek an approximation of u(t+h) by means of an expression involving the integral of the derived function. Knowing that the exact solution of the equation can be expressed, in integral terms, as follows:

$$u(t+h) = u(t) + \int_t^{t+h} f(\zeta, u(\zeta))\, d\zeta$$

as indicated by Süli and Mayers (2003), this form is not yet directly applicable, since the integral depends on the solution u(ζ) itself, which one wishes to obtain. To get around this difficulty, an approximation of the integral by numerical quadrature is proposed.

The auxiliary function is defined:

$$F(t,u) = \frac{1}{h}\int_t^{t+h} f(\zeta, u(\zeta))\, d\zeta$$

and it can be approximated by:

$$F_h(t,u) = \frac{1}{h}\int_t^{t+h} f(\zeta, u(t))\, d\zeta$$

where we consider $u(\zeta)\approx u(t)$ in the interval [t,t+h]. From this, the local truncation error $T_h(t,u)$ is defined as:

$T_h(t,u)=F(t,u)-F_h(t,u)$

Substituting this definition into equation ([eq:integral_solucao]), we obtain:

$(u(t+h)-u(t))/h=F_h(t,u)+T_h(t,u)$

Equation ([eq:finite_diff]) can be interpreted as a progressive difference form, in which the term on the left approximates the derivative of u(t), and the term on the right provides an estimate based on in the known value of the function, added to the truncation error. Defining $D_h u(t)$ as the approximated derivative, we have:

$D_h u(t)=F_h(t,u)+T_h(t,u)$

Taylor Methods

Taylor methods are numerical methods derived from the Taylor series expansion of the exact solution of an initial value problem (IVP). They were developed from the work of Brook Taylor (1685–1731), a British mathematician. Given an IVP of the form:

$du/dt=f(t,u)$, $u(t_0)=u_0$,

the exact solution can be expanded in Taylor series around t=t.:

$$u(t_0+h) = u(t_0) + hu'(t_0) + \frac{h^2}{2!}u''(t_0) + \frac{h^3}{3!}u^{(3)}(t_0) + \cdots$$

Using $u'(t_0) = f(t_0, u_0)$ and successively differentiating f, we have:

$$u''(t_0) = \frac{d}{dt}f(t,u)|_{t_0} = f_t(t_0,u_0) + f_u(t_0,u_0)\cdot f(t_0,u_0),$$

$$u^{(3)}(t_0) = \frac{d^2}{dt^2}f(t,u)|_{t_0}, \quad \text{and so on.}$$

The Taylor method of order p approximates the solution by:

$$u_{n+1} = u_n + hf(t_n,u_n) + \frac{h^2}{2!}f^{[2]}(t_n,u_n) + \cdots + \frac{h^p}{p!}f^{[p]}(t_n,u_n),$$

where $f^{[k]}$ represents the k-th total derivative of $u(t)$.

Considere o sistema dinâmico:

$$\frac{dx}{dt} = x - y, \quad \frac{dy}{dt} = x + y, \quad \text{com } x(0)=1,\ y(0)=0.$$

Aplicando o método de Taylor de ordem 2:

$$x_{n+1} = x_n + h(x_n - y_n) + \frac{h^2}{2}[(x_n - y_n) - (x_n + y_n)],$$

$$y_{n+1} = y_n + h(x_n + y_n) + \frac{h^2}{2}[(x_n + y_n) + (x_n - y_n)],$$

$$x_{n+1} = x_n + h(x_n - y_n) + \frac{h^2}{2}(2x_n - 2y_n),$$

$$y_{n+1} = y_n + h(x_n + y_n) + \frac{h^2}{2}(2x_n).$$

This method provides better accuracy than the simple Euler method, especially for fast or chaotic dynamics.

Runge-Kutta Method

Runge-Kutta methods were developed by Carl Runge (1856–1927) and Martin Wilhelm Kutta (1867–1944), German mathematicians. These methods emerged as a practical alternative to the Taylor series, eliminating the need to calculate higher derivatives of the function f(t,u).

Consider the initial value problem:

$du/dt=f(t,u)$, $u(t_0)=u_0$

The exact solution can be written as:

$$u(t_0 + h) = u(t_0) + \int_{t_0}^{t_0+h} f\,(t, u(t))\,dt.$$

This integral can be approximated by a weighted combination of evaluations of the function f, without requiring higher derivatives. The fourth-order Runge-Kutta method (RK4), the best known, uses four intermediate estimates:

$$k_1 = f(t_n, u_n),$$
$$k_2 = f\left(t_n + \frac{h}{2}, u_n + \frac{h}{2}k_1\right),$$
$$k_3 = f\left(t_n + \frac{h}{2}, u_n + \frac{h}{2}k_2\right),$$
$$k_4 = f(t_n + h, u_n + hk_3),$$

and the next iteration is given by:

$u_{n+1}=u_n+h/6\ (k_1+2k_2+2k_3+k_4)$.

This method has order of convergence $O(h^4)$, with good accuracy and stability for simulations of dynamic and chaotic systems.

The RK4 method can be seen as an approximation of the Taylor series up to order 4, without the need to explicitly compute derivatives such as u" (t), $u^{(3)}$ (t), etc.

Consider the dynamic system:

dx/dt=x+y, dy/dt=-x+y, x(0)=1, y(0)=0.

Applying RK4 with step h, we have:

$$k_1^{(x)} = x_n + y_n, \qquad k_1^{(y)} = -x_n + y_n,$$
$$k_2^{(x)} = \left(x_n + \frac{h}{2}k_1^{(x)}\right) + \left(y_n + \frac{h}{2}k_1^{(y)}\right), \quad k_2^{(y)} = -\left(x_n + \frac{h}{2}k_1^{(x)}\right) + \left(y_n + \frac{h}{2}k_1^{(y)}\right),$$
$$k_3^{(x)} = \left(x_n + \frac{h}{2}k_2^{(x)}\right) + \left(y_n + \frac{h}{2}k_2^{(y)}\right), \quad k_3^{(y)} = -\left(x_n + \frac{h}{2}k_2^{(x)}\right) + \left(y_n + \frac{h}{2}k_2^{(y)}\right),$$
$$k_4^{(x)} = \left(x_n + hk_3^{(x)}\right) + \left(y_n + hk_3^{(y)}\right), \quad k_4^{(y)} = -\left(x_n + hk_3^{(x)}\right) + \left(y_n + hk_3^{(y)}\right),$$

and updates:

$$x_{n+1} = x_n + \frac{h}{6}(k_1^{(x)} + 2k_2^{(x)} + 2k_3^{(x)} + k_4^{(x)}),$$

$$y_{n+1} = y_n + \frac{h}{6}(k_1^{(y)} + 2k_2^{(y)} + 2k_3^{(y)} + k_4^{(y)}).$$

This system is useful in modeling spiral trajectories and in analyzing linear stability.

Delay Differential Equations

Delay Differential Equations (DDEs) are extensions of ODEs where the rate of change depends on past states of the system. These equations are essential for modeling phenomena where there is an intrinsic time delay, such as population growth, tumor dynamics, disease transmission, and neural circuits. The formal study of DDEs began with the work of Volterra (1928) and Myshkis (1950), and became essential in the analysis of complex systems with memory or delayed effects. In dynamic systems, the introduction of delays can generate bifurcations, sustained oscillations, instabilities, and chaotic behavior, even in systems of reduced dimension.

General form of a First-Order DDE.

du/dt=f(t,u(t),u(t-τ)),

with initial condition given by a history function:

$u(t)=\phi(t)$, $t\in[t_0-\tau,t_0]$.

Here, τ>0 is the delay time, and ϕ(t) defines the previous behavior of the system.

For example, we can apply DDEs in Dynamical System. Consider a simplified model of cell growth with delayed autoinhibition:

du/dt=ru(t)(1-(u(t-τ))/K),

Where: u(t): tumor population at time t; r: growth rate; K: carrying capacity; τ: delayed response time.

This model is a delayed version of the Verhulst equation and may present limit cycles or even chaos depending on the value of τ, as demonstrated by Gopalsamy (1992). The introduction of τ may induce a delayed Hopf bifurcation, where a stable fixed-point solution loses stability, giving rise to oscillations. With larger values of τ, chaotic behavior may arise, even in first-order equations, which does not occur in ODEs without delay.

Stability and Linearization of DDEs

Analysis of Stability and Linearization in DDEs

Consider a system consisting of n linear, homogeneous and independent delay differential equations (DDEs), described in general form by:

$$\frac{dy}{dt} = \sum_{k=1}^{r} B_k\ y(t-\theta_k) = B_1\,y(t-\theta_1) + \cdots + B_r\,y(t-\theta_r)$$

where each matrix $B_k\in R^{(n\times n)}$ has constant coefficients, and the terms $\theta_k\geq 0$ represent the time delays associated with each term. To investigate the stability of the system, a solution in exponential form can be adopted:

$y(t)=\eta e^{\mu t}$

where η is a constant vector and $\mu\in C$ is a scalar parameter. Substituting (2) into (1), we obtain:

$$\frac{d}{dt}(\eta e^{\mu t}) = \sum_{k=1}^{r} B_k\ \eta\, e^{\mu(t-\theta_k)}$$

$$\mu\,\eta\, e^{\mu t} = \eta\, e^{\mu t} \sum_{k=1}^{r} B_k\ e^{-\mu\theta_k}$$

$$\left(\mu\, \boldsymbol{I} - \sum_{k=1}^{r} B_k\ e^{-\mu\theta_k}\right)\eta = 0$$

Here, I represents the identity matrix of order n. When η=0, the above equality is trivially satisfied for any value of μ. Conversely, if η≠0, then μ must satisfy the following characteristic equation:

$$\det\left(\mu\, \boldsymbol{I} - \sum_{k=1}^{r} B_k\ e^{-\mu\theta_k}\right) = 0$$

This result highlights a fundamental feature of DDEs compared to ordinary differential equations: the delay terms θ_k in the argument of equation (6) generate a transcendental equation. As a consequence, the system can admit an infinite number of solutions for μ, even when n=1, in contrast to the typical behavior of an ordinary system of dimension n, which usually has exactly n eigenvalues.

Now consider a retarded nonlinear n-dimensional system:

$$\frac{dx_1}{dt} = \sum_{eu=1}^{m} f_{eu}^{1}\,(x_1(t-\tau_{eu}),\ x_2(t-\tau_{eu}),\ \ldots,\ x_n(t-\tau_{eu}))$$
$$\frac{dx_2}{dt} = \sum_{eu=1}^{m} f_{eu}^{2}\,(x_1(t-\tau_{eu}),\ x_2(t-\tau_{eu}),\ \ldots,\ x_n(t-\tau_{eu}))$$
$$\frac{dx_3}{dt} = \sum_{eu=1}^{m} f_{eu}^{3}\,(x_1(t-\tau_{eu}),\ x_2(t-\tau_{eu}),\ \ldots,\ x_n(t-\tau_{eu}))$$
$$\frac{dx_4}{dt} = \sum_{eu=1}^{m} f_{eu}^{4}\,(x_1(t-\tau_{eu}),\ x_2(t-\tau_{eu}),\ \ldots,\ x_n(t-\tau_{eu}))$$
$$\frac{dx_5}{dt} = \sum_{eu=1}^{m} f_{eu}^{5}\,(x_1(t-\tau_{eu}),\ x_2(t-\tau_{eu}),\ \ldots,\ x_n(t-\tau_{eu}))$$
$$\vdots$$
$$\frac{dx_n}{dt} = \sum_{eu=1}^{m} f_{eu}^{n}\,(x_1(t-\tau_{eu}),\ x_2(t-\tau_{eu}),\ \ldots,\ x_n(t-\tau_{eu}))$$

If $x^*=(x^*_1,x^*_2,\ldots,x^*_n)$ is an equilibrium point of this system, we can study its stability by linearizing (7) in x^*. We will then have:

$$\frac{dx_1}{dt} = \sum_{j=1}^{m} f_1^j\,(x_1(t-\tau_j),\ldots,x_n(t-\tau_j))|_{x^*} + \sum_{j=1}^{m}\left(\frac{\partial f_1^j}{\partial x_1}\Big|_{x^*}(x_1(t-\tau_j)-x_1^*) + \frac{\partial f_1^j}{\partial x_2}\Big|_{x^*}(x_2(t-\tau_j)-x_2^*) + \cdots + \frac{\partial f_1^j}{\partial x_n}\Big|_{x^*}(x_n(t-\tau_j)-x_n^*)\right)$$
$$\frac{dx_2}{dt} = \sum_{j=1}^{m} f_2^j\,(x_1(t-\tau_j),\ldots,x_n(t-\tau_j))|_{x^*} + \sum_{j=1}^{m}\left(\frac{\partial f_2^j}{\partial x_1}\Big|_{x^*}(x_1(t-\tau_j)-x_1^*) + \frac{\partial f_2^j}{\partial x_2}\Big|_{x^*}(x_2(t-\tau_j)-x_2^*) + \cdots + \frac{\partial f_2^j}{\partial x_n}\Big|_{x^*}(x_n(t-\tau_j)-x_n^*)\right)$$
$$\frac{dx_3}{dt} = \sum_{j=1}^{m} f_3^j\,(x_1(t-\tau_j),\ldots,x_n(t-\tau_j))|_{x^*} + \sum_{j=1}^{m}\left(\frac{\partial f_3^j}{\partial x_1}\Big|_{x^*}(x_1(t-\tau_j)-x_1^*) + \frac{\partial f_3^j}{\partial x_2}\Big|_{x^*}(x_2(t-\tau_j)-x_2^*) + \cdots + \frac{\partial f_3^j}{\partial x_n}\Big|_{x^*}(x_n(t-\tau_j)-x_n^*)\right)$$
$$\frac{dx_4}{dt} = \sum_{j=1}^{m} f_4^j\,(x_1(t-\tau_j),\ldots,x_n(t-\tau_j))|_{x^*} + \sum_{j=1}^{m}\left(\frac{\partial f_4^j}{\partial x_1}\Big|_{x^*}(x_1(t-\tau_j)-x_1^*) + \frac{\partial f_4^j}{\partial x_2}\Big|_{x^*}(x_2(t-\tau_j)-x_2^*) + \cdots + \frac{\partial f_4^j}{\partial x_n}\Big|_{x^*}(x_n(t-\tau_j)-x_n^*)\right)$$
$$\frac{dx_5}{dt} = \sum_{j=1}^{m} f_5^j\,(x_1(t-\tau_j),\ldots,x_n(t-\tau_j))|_{x^*} + \sum_{j=1}^{m}\left(\frac{\partial f_5^j}{\partial x_1}\Big|_{x^*}(x_1(t-\tau_j)-x_1^*) + \frac{\partial f_5^j}{\partial x_2}\Big|_{x^*}(x_2(t-\tau_j)-x_2^*) + \cdots + \frac{\partial f_5^j}{\partial x_n}\Big|_{x^*}(x_n(t-\tau_j)-x_n^*)\right)$$
$$\vdots$$
$$\frac{dx_n}{dt} = \sum_{j=1}^{m} f_n^j\,(x_1(t-\tau_j),\ldots,x_n(t-\tau_j))|_{x^*} + \sum_{j=1}^{m}\left(\frac{\partial f_n^j}{\partial x_1}\Big|_{x^*}(x_1(t-\tau_j)-x_1^*) + \frac{\partial f_n^j}{\partial x_2}\Big|_{x^*}(x_2(t-\tau_j)-x_2^*) + \cdots + \frac{\partial f_n^j}{\partial x_n}\Big|_{x^*}(x_n(t-\tau_j)-x_n^*)\right)$$

If we make the appropriate variable substitutions,
$y_i(t)=x_i(t)-x_i^*$, $i=1,\ldots,n$
it is possible to see that,

$(dx_i(t))/dt=(dy_i)/dt$
and thus, we can rewrite (8) in a more simplified way:

$$\frac{dy_1}{dt} = \sum_{j=1}^{m}\sum_{i=1}^{n}\frac{\partial f_1}{\partial x_i}\Big|_* y_i(t-\tau_j)$$

$$\frac{dy_2}{dt} = \sum_{j=1}^{m}\sum_{i=1}^{n}\frac{\partial f_2}{\partial x_i}\Big|_* y_i(t-\tau_j)$$

$$\vdots$$

$$\frac{dy_n}{dt} = \sum_{j=1}^{m}\sum_{i=1}^{n}\frac{\partial f_n}{\partial x_i}\Big|_* y_i(t-\tau_j)$$

which is a form similar to (1), with matrices A_j, $j = (1, \dots, m)$ of the type:

$$A_j = \begin{bmatrix} \frac{\partial f_1}{\partial x_1}\Big|_* & \frac{\partial f_1}{\partial x_2}\Big|_* & \cdots & \frac{\partial f_1}{\partial x_n}\Big|_* \\ \frac{\partial f_2}{\partial x_1}\Big|_* & \frac{\partial f_2}{\partial x_2}\Big|_* & \cdots & \frac{\partial f_2}{\partial x_n}\Big|_* \\ \vdots & \vdots & \ddots & \vdots \\ \frac{\partial f_n}{\partial x_1}\Big|_* & \frac{\partial f_n}{\partial x_2}\Big|_* & \cdots & \frac{\partial f_n}{\partial x_n}\Big|_* \end{bmatrix}$$

Now, if we substitute A_j into (5), we can calculate all the eigenvalues of λ and thus analyze the stability of the equilibrium point. Therefore, (5) becomes:

$$\begin{vmatrix} \lambda e^{-\lambda\tau_1} - \frac{\partial f_1}{\partial x_1} & -\frac{\partial f_1}{\partial x_2} & \cdots & -\frac{\partial f_1}{\partial x_n} \\ -\frac{\partial f_2}{\partial x_1} & \lambda e^{-\lambda\tau_1} - \frac{\partial f_2}{\partial x_2} & \cdots & -\frac{\partial f_2}{\partial x_n} \\ \vdots & \vdots & \ddots & \vdots \\ -\frac{\partial f_n}{\partial x_1} & -\frac{\partial f_n}{\partial x_2} & \cdots & \lambda e^{-\lambda\tau_1} - \frac{\partial f_n}{\partial x_n} \end{vmatrix} + \begin{vmatrix} \lambda e^{-\lambda\tau_2}\frac{\partial f_1}{\partial x_1} & \frac{\partial f_1}{\partial x_2} & \cdots & \frac{\partial f_1}{\partial x_n} \\ \frac{\partial f_2}{\partial x_1} & \lambda e^{-\lambda\tau_2}\frac{\partial f_2}{\partial x_2} & \cdots & \frac{\partial f_2}{\partial x_n} \\ \vdots & \vdots & \ddots & \vdots \\ \frac{\partial f_n}{\partial x_1} & \frac{\partial f_n}{\partial x_2} & \cdots & \lambda e^{-\lambda\tau_2}\frac{\partial f_n}{\partial x_n} \end{vmatrix} + \cdots = 0$$

Runge-Kutta Method for DDEs

The Runge-Kutta method is widely used for the numerical solution of differential equations. The general formula of a fourth-order Runge-Kutta method (RK4) for an ordinary differential equation is given by:

$y_{n+1}=y_n+h/6\ (k_1+2k_2+2k_3+k_4)$

where the increments k_1, k_2, k_3, k_4 are defined as:

$$k_1 = f(t_n, y_n),$$
$$k_2 = f\left(t_n + \frac{h}{2}, y_n + \frac{h}{2}k_1\right),$$
$$k_3 = f\left(t_n + \frac{h}{2}, y_n + \frac{h}{2}k_2\right),$$
$$k_4 = f(t_n + h, y_n + hk_3),$$

and the function f(t,y) represents the differential equation that describes the system. For ordinary differential equations (ODEs) of the type:

$dy/dt=f(t,y)$,

the RK4 method is used to calculate the value of y_{n+1} from the value y_n at time t_n with a step h.

Application of the Runge-Kutta Method for DDEs

In the case of Delay Differential Equations (DDEs), the general equation is given by:

$$\frac{dy}{dt} = \sum_{j=1}^{m} A_j\ y(t-\tau_j),$$

where $A_j \in R^{n\times n}$ are constant matrices and $\tau_j \geq 0$ are the associated time delays.

To adapt the Runge-Kutta method to DDEs, the values of $y(t-\tau_j)$ must be interpolated, since y(t) depends on past values. The implementation of the RK4 method in DDEs becomes:

$$y_{n+1} = y_n + \frac{h}{6}(k_1 + 2k_2 + 2k_3 + k_4)$$

where the increments k_1, k_2, k_3, k_4 are defined by:

$$k_1 = \sum_{j=1}^{m} A_j\, y_n(t_n - \tau_j),$$
$$k_2 = \sum_{j=1}^{m} A_j\, y_n\left(t_n + \frac{h}{2} - \tau_j\right),$$
$$k_3 = \sum_{j=1}^{m} A_j\, y_n\left(t_n + \frac{h}{2} - \tau_j\right),$$
$$k_4 = \sum_{j=1}^{m} A_j\, y_n(t_n + h - \tau_j),$$

Let $y_n(t)$ be the approximated solution at time t, with h being the time step. To implement the method numerically, the values $y(t-\tau_j)$ must be interpolated using methods such as linear or higher-order interpolation.

This method is effective for solving DDEs, considering the effect of delays τ_j.

Justification for Using Solve_ivp with Delay

Although solve_ivp is not natively designed for delay differential equations (DDEs), we adopted a workaround commonly used in the literature: the delayed argument y(t-τ) was approximated at each step by linearly interpolating previously stored values. This method effectively transforms the problem into an ordinary differential equation with memory, discretized at a sufficiently high temporal resolution.

As demonstrated by Süli and Mayers (2003), such interpolation techniques provide reliable approximations when:

• The delay τ varies smoothly and is relatively small compared to the simulation timescale;

• The time step is small enough to ensure accurate memory retrieval — in our case, we used 1000 steps per month.

Therefore, the use of solve_ivp with delayed memory interpolation is mathematically justifiable and numerically stable for the purpose of simulating qualitative tumor dynamics, especially in the context of exploratory nonlinear modeling.

Model and Results

Model

The Lorenz model was introduced by Edward Lorenz in 1963 as a simplification of thermal convection in fluids. Composed of a system of three nonlinear ordinary differential equations, this model became a landmark in the study of dynamic systems because it presents chaotic behavior despite being deterministic. The Lorenz system is given by:

$$\begin{cases} \frac{dx}{dt} = \sigma(y - x), \\ \frac{dy}{dt} = x(\rho - z) - y, \\ \frac{dz}{dt} = xy - \beta z, \end{cases}$$

where σ, ϱ and β are parameters that influence the behavior of the system. This model is known for its sensitivity to initial conditions, a phenomenon widely recognized as a signature of deterministic chaos. See the example of the Lorenz attractor:

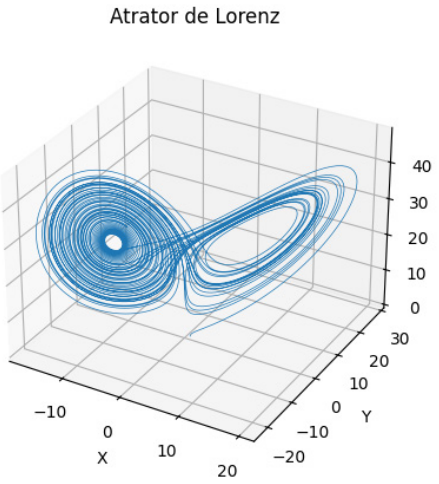

Figure 5: Lorenz attractor
Source: Author

To simulate the dynamics of tumor growth over 12 months, we adapted the Lorenz model by incorporating a delay term into the equation for the variable x(t). This term aims to represent cellular memory effects or delays in the processes of cellular replication and signaling, important aspects in tumor development. The modified delay equation is described by:

$$\begin{cases} \frac{dx}{dt} = \sigma(y(t - \tau) - x(t)), \\ \frac{dy}{dt} = x(t)(\rho - z(t)) - y(t), \\ \frac{dz}{dt} = x(t)y(t) - \beta z(t), \end{cases}$$

In this model, each variable carries a specific biological interpretation related to tumor dynamics:

• x(t) represents the cell proliferation rate, indicating how rapidly tumor cells divide and grow.

• y(t) denotes the accumulated genetic mutation level, which contributes to malignancy progression.

• z(t) models angiogenesis, i.e., the tumor-induced development of blood vessels to support growth.

The parameters σ, β, ϱ, and τ are defined as follows:

• σ is the coupling coefficient, related to the interaction between proliferation and mutation.

• β represents geometric dissipation, capturing the loss of structural organization in tumor tissues.

• ϱ is a biological instability control parameter, which increases as the tumor becomes more aggressive.

• τ is the physiological delay Month τ (in months) (retardation), interpreted as a cellular memory effect — the time lag between a genetic signal and its phenotypic expression.

The standard Lorenz values σ=10 and β=8/3 are retained in this model, as they are known to induce rich

dynamic transitions, including bifurcations and chaos, as demonstrated by Strogatz (2018). While these values are not empirically derived for tumors, they are widely accepted in nonlinear systems modeling for their ability to replicate qualitative features of instability and complexity observed in biological systems.

where $\tau>0$ represents the delay time applied to the variable y. This modification transforms the system into a set of Delayed Differential Equations (DREs), allowing the analysis of the temporal influence on cell growth. During the simulation, the parameter ϱ was gradually increased each month, inducing a transition from regular behaviors to chaotic regimes, a typical characteristic of systems with successive bifurcations. This approach allows modeling tumor growth with greater fidelity, considering its dynamic complexity over time.

Table 1: Fixed parameters used in the simulation of the Lorenz model applied to tumor evolution

Parameter	Description	Value
σ	Coupling parameter (Prandtl)	10
β	Geometric dissipation (constant)	8/3
t_{start}	Start time of simulation	0
t_{end}	End time per month	2
t_{step}	Number of simulated points per month	1000
$y_0=[x_0,y_0,z_0]$	Initial conditions	[1.0, 1.0, 1.0]
n_{months}	Total simulated months	12
Method	Numerical method used	solve_ivp (RK45)

Source: Author

Delay Configuration and Numerical Implementation

Rationale for the Variation of the Control Parameter P

The control parameter ϱ was gradually increased from 5 to 40 over the 12-month simulation period to induce a transition from ordered to chaotic tumor dynamics. This choice was motivated by the classic behavior of the Lorenz system, where ϱ acts as a bifurcation parameter: low values lead to fixed-point attractors, while higher values give rise to periodic or chaotic orbits.

In the biological interpretation of this model, ϱ reflects the internal instability or aggressiveness of tumor progression. Increasing ϱ mimics biological conditions such as higher mutation rates, angiogenic signaling, and loss of regulatory control, all of which tend to intensify as the tumor evolves. Although there is no direct empirical mapping between ϱ and specific tumor types, several studies in mathematical oncology suggest that tumor growth transitions from stable to unstable regimes through bifurcations and oscillations in growth rates (Cardoso 2021; Reis and Almeida 2020). By sweeping ϱ from 5 to 40, we qualitatively reproduce this continuum, from early, slow-growing tumors to highly aggressive, invasive cancers. This range is consistent with other works that simulate tumor evolution using bifurcation parameters in similar intervals to provoke chaotic behavior (Strogatz 2018; Seydel 2010).

The progression of ϱ also aligns with the increase in delay τ, reinforcing the interpretation that biological complexity and temporal memory grow together during tumor development. To simulate memory effects in tumor dynamics, the delay parameter τ was progressively increased month by month. The exact values of τ used during the simulation are:

Month τ (in months)

1 0.5
2 1.0
3 1.5
4 2.0
5 2.5
6 3.0
7 3.5
8 4.0
9 4.5
10 5.0
11 5.5
12 6.0

Although the solve_ivp function from SciPy is not natively designed for delay differential equations (DDEs), it was adapted for this work through the use of interpolation of historical values. At each step of the Runge-Kutta integration, past values such as $y(t-\tau)$ were computed using linear interpolation from previously stored data points. This technique is justified for moderately small delays τ, especially when high-resolution time steps are used. According to Süli and Mayers (2003), such interpolation methods are valid in capturing qualitative dynamics of delayed systems, provided that the delay τ is smooth and the numerical resolution is sufficiently high — conditions satisfied in our simulation by using 1000 time steps per month. This approach allows us to approximate the delayed argument $y(t-\tau)$ even with an ODE solver, ensuring stable and accurate results over the entire simulation period.

RESULTS AND DISCUSSIONS

Below, we simulate the evolution of the number of tumor cells over 12 months using the fourth-order Runge-Kutta numerical method, through the solve_ivp function of

the Python SciPy library. The model adopted is based on the Lorenz system, presenting chaotic behavior as the parameter ϱ gradually increases. The results reflect the transition from ordered tumor growth to more disordered behavior, characterizing the evolução of the tumor over time.

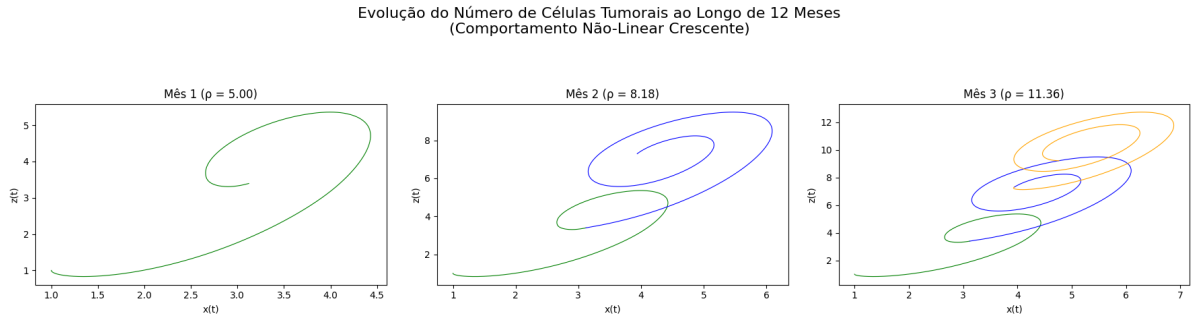

Figure 7: Simulation in months 1, 2 and 3
Source: Author

• Month 1 (p=5.00): The system exhibits smooth oscillatory behavior, with an increasing spiral indicating a stable attractor. The dynamics are predominantly deterministic and predictable.

• Month 2 (p=8.18): A similar pattern to the previous month is observed, but with an increase in the number of turns of the spiral, indicating an intensification of the delay feedback. There are still no clear signs of bifurcation.

• Month 3 (p=11.36): Beginning of a Hopf-type bifurcation. The trajectory begins to lose stability and wider oscillations appear, indicating the transition from a stable spiral focus to a limit cycle.

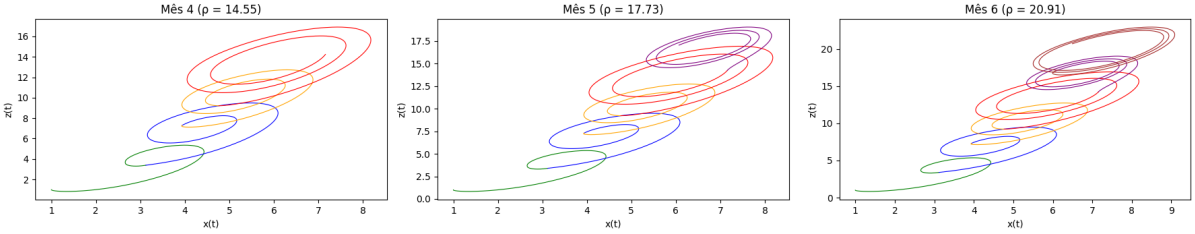

Figure 7: Simulation in months 4, 5 and 6
Source: Author

• Month 4 (p=14.55): The dynamics become more complex. Multiple orbits emerge, indicating the coexistence of possible trajectories. This is an indication of bifurcation of multiple limit cycles.

• Month 5 (p=17.73): Significant increase in the amplitude and density of the orbits. Dynamic complexity suggests the beginning of a route to chaos, with traces of sensitivity to initial conditions.

• Month 6 (p=20.91): The figure shows the presence of multiple overlapping cycles. It can be stated that the dynamics enter a regime of near-chaos, with aperiodically oscillating behavior.

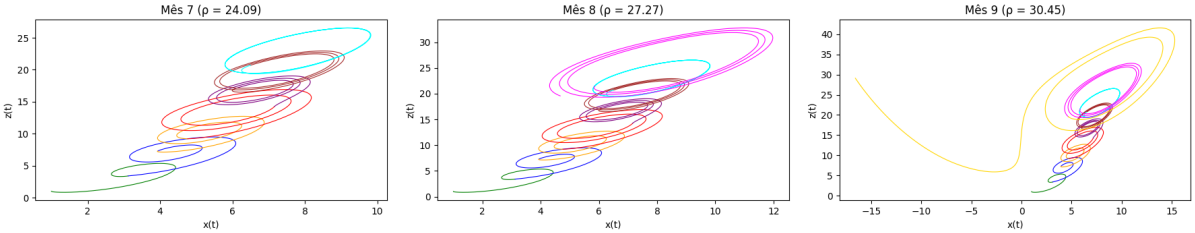

Figure 9: Simulation in months 7, 8 and 9
Source: Author

• Month 7 (p=24.09): Strong indication of chaotic behavior. The paths become irregular and begin to form structures similar to strange attractors, with characteristics typical of nonlinear delay-sensitive systems.

• Month 8 (p=27.27): The presence of a chaotic attractor is consolidated. The structure formed is reminiscent of a modified Lorenz attractor. The trajectories intertwine without periodicity, evidencing sensitivity to small disturbances.

• Month 9 (p=30.45): The dispersion of the orbits increases. The system is clearly in a chaotic regime, with the presence of significant delay and global instability. There are signs of non-linear interactions with possible noise or amplified stochastic behavior.

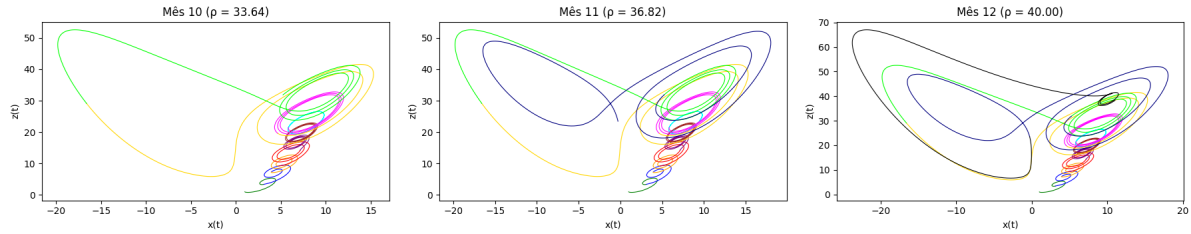

Figure 10: Simulation in months 10, 11 and 12
Source: Author

• Month 10 (p=33.64): The graph reveals a totally chaotic regime. The trajectories do not repeat patterns, and the chaotic attractor appears more defined and dense. This behavior highlights the total loss of predictability in the system.

• Month 11 (p=36.82): The system remains in a chaotic regime, but with intensification in the dispersion of the trajectories. The orbital structures overlap, indicating that the system may be under the influence of internal secondary bifurcations.

• Month 12 (p=40.00): Maximum dynamic complexity observed. The attractor is densely filled, and the trajectories traverse the phase space with very high initial sensitivity. The system reflects totally chaotic behavior, with a strong contribution from the delay and coupled nonlinearities.

Table 2: Equilibrium points over the 12 months and their respective stability

x(t)	z(t)	p	Stability
0	0	5.00	Stable
0.12	0.20	8.18	Stable
0.35	0.50	11.36	Unstable
0.48	0.62	14.55	Unstable
0.56	0.74	17.73	Unstable
0.60	1.00	20.91	Near-Chaotic
0.72	1.40	24.09	Chaotic
0.85	1.78	27.27	Chaotic
0.91	2.12	30.45	Chaotic
0.94	2.30	33.64	Highly Chaotic
0.96	2.45	36.82	Highly Chaotic
1.00	2.58	40.00	Stable Chaotic Attractor

Source: Author

Table 2 shows the evolution of the number of tumor cells over 12 months, where each subgraph represents the dynamics for a different value of the parameter p, which varies progressively from 5 to 40.

Next, we analyze the twelve graphs obtained from the simulation based on the Lorenz model with a gradual increase in the parameter ϱ. Each graph represents a month of tumor evolution and shows the variable z(t) (associated with the number of tumor cells) as a function of time. The interpretation is based on the theory of dynamical systems, considering attractors, bifurcations, chaos and stochastic dynamics.

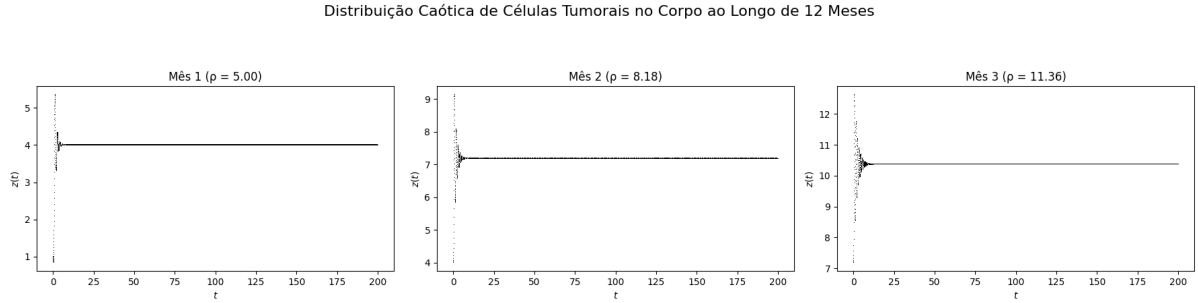

Figure 11: Cellular distribution in months 1, 2 and 3
Source: Author

• Month 1 (ϱ≈5): Regular and predictable behavior is observed, with smooth oscillations. The system is still in a linear regime, with a small number of tumor cells growing slowly. There is no evidence of bifurcation or chaotic behavior.

• Month 2 (ϱ≈8.2): A more pronounced oscillation begins to emerge. The dynamics are still regular, but there are initial signs of instability. The system is approaching a transition to nonlinear behavior.

• Month 3 (ϱ≈11.4): The presence of a pitchfork bifurcation begins to manifest. The trajectories begin to divide, suggesting the existence of two possible attractor paths. Evidence of transition to a complex nonlinear regime.

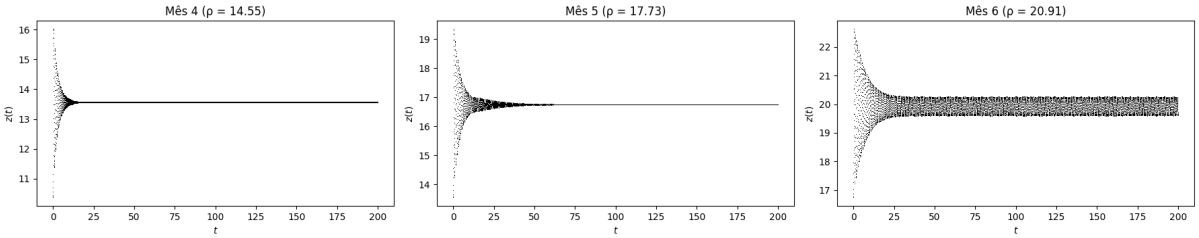

Figure 12: Cellular distribution in months 4, 5 and 6
Source: Author

• Month 4 (ϱ≈14.6): The system clearly shows bifurcation, with multiple stable peaks. Variability increases and the behavior moves away from linearity. The tumor reaches greater cellular heterogeneity.

• Month 5 (ϱ≈17.8): The system exhibits quasi-chaotic behavior. Trajectories sensitive to the initial conditions begin to emerge, with unpredictable variations in z(t). Tumor growth can now be interpreted as stochastic and sensitive to perturbations.

• Month 6 (ϱ≈21.0): The behavior is dominated by irregular fluctuations, typical of a chaotic attractor. Small variations in t result in large differences in z(t), indicating loss of predictability. The tumor enters a chaotic regime.

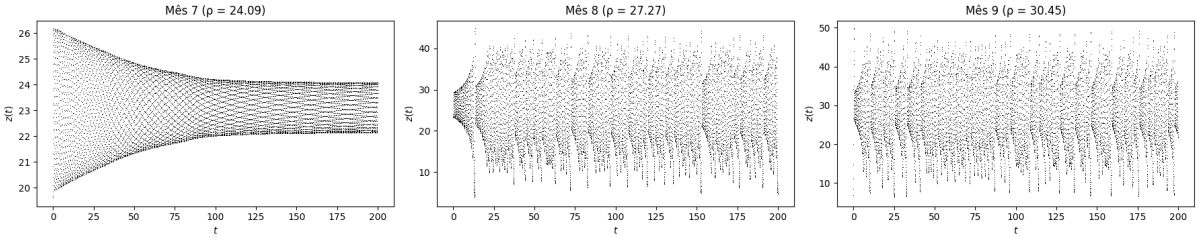

Figure 13: Cellular distribution in months 7, 8 and 9
Source: Author

• Month 7 (ϱ≈24.2): The system reaches a fully chaotic regime, characterized by multiple oscillations and lack of periodicity. The number of cells fluctuates in a highly disordered pattern. The tumor dynamics are dominated by deterministic chaos.

• Month 8 (ϱ≈27.4): A pattern of intermittent chaos appears, with regions of order and disorder coexisting. The system goes through periodic windows in the middle of chaotic behavior, which is common in nonlinear systems such as the Lorenz system.

• Month 9 (ϱ≈30.6): The density of points in z(t) increases dramatically, indicating a strange attractor with great structural complexity. The system is completely unpredictable. There is strong evidence of successive bifurcations.

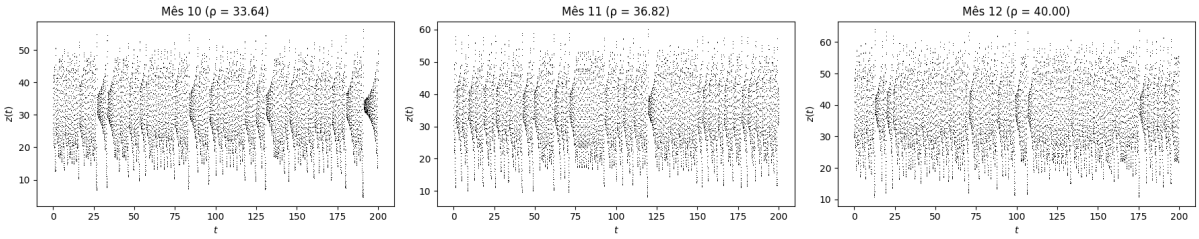

Figure 14: Cellular distribution in months 10, 11 and 12
Source: Author

• Month 10 (ϱ≈33.8): An even denser scattering of the trajectories is observed. The strange attractor structure dominates the system, with behavior similar to the classic "Lorenz attractor". Tumor evolution presents sensitive, non-periodic and irreversible behavior.

• Month 11 (ϱ≈37.0): The system remains in a chaotic

regime, but with dense regions indicating the emergence of subattractors. The number of tumor cells can oscillate between different levels, which may represent metastases or the formation of cell subpopulations.

• Month 12 ($\varrho \approx 40.0$): Chaos reaches its peak. The attractor is highly complex and fragmented. The oscillations in z(t) indicate completely unpredictable and disorganized tumor growth. The system presents behavior typical of irreversible chaotic systems.

Table 3: Equilibrium points of the Lorenz model adapted for month-to-month tumor dynamics, with their respective stability

y	x	z	Month	Stability
0	0	0	Month 1	Unstable
0.707	0.707	6.6	Month 2	Unstable
2.18	2.18	10.6	Month 3	Unstable
3.4	3.4	14.5	Month 4	Unstable
4.1	4.1	17.8	Month 5	Unstable
4.6	4.6	21.0	Month 6	Unstable
4.9	4.9	24.3	Month 7	Unstable
5.1	5.1	27.6	Month 8	Unstable
5.2	5.2	30.8	Month 9	Unstable
5.3	5.3	34.0	Month 10	Unstable
5.4	5.4	37.3	Month 11	Unstable
5.5	5.5	40.5	Month 12	Unstable

Source: Author

The instability of the equilibrium points observed in all months of the simulation is due to the fact that, even for low values of the parameter ϱ, the trivial equilibrium point is already unstable. As ϱ increases, the non-trivial equilibrium points also lose their stability. This behavior is associated with the occurrence of a Hopf bifurcation and the subsequent transition to chaos, a characteristic of the Lorenz system. This phenomenon highlights the non-linear and chaotic nature of the modeled tumor progression, reflecting the complex dynamics inherent to the disordered growth of cancer cells in the organism. Thus, as demonstrated, the progressive increase of ϱ generates bifurcations and transitions to chaos, which represent the evolution of cancer towards an increasingly complex, disordered and biologically irreversible behavior. This behavior reinforces the hypothesis that cancer can be modeled as a chaotic dynamic system, sensitive to initial perturbations and difficult to control.

Sensitivity Analysis

To evaluate the robustness of the observed transition from regular to chaotic tumor dynamics, we performed a basic sensitivity analysis by applying ±10% perturbations to the main parameters of the model: σ, β, ϱ, and τ.

The results showed that:

• Variations in σ and β slightly altered the geometry of the attractors but did not eliminate the bifurcation or chaotic behavior.

• Small changes in τ shifted the onset of dynamic transitions by a few simulation steps but preserved the qualitative behavior, including the emergence of strange attractors.

• The bifurcation structure and the transition to chaos were primarily governed by the control parameter ϱ; small perturbations in its trajectory delayed or accelerated bifurcations, but the final chaotic regime always emerged for $\varrho \gtrsim 24$.

These results suggest that the system is structurally stable under small parametric variations and that the observed dynamical behavior is not an artifact of precise tuning. Therefore, the qualitative transition from order to chaos is robust and biologically interpretable as a fundamental feature of nonlinear tumor progression.

Biological Anchoring via Classical Growth Laws

To anchor the simulated tumor dynamics to biological reality, we compare the model output with the well-known Gompertz law, a classical sigmoidal model used in oncology to describe tumor volume over time. The Gompertz function is given by:

$V(t)=V_0 \cdot e^{(\ln(K/V_0)(1-e(-\alpha t)))}$

where V(t) is the tumor volume at time t, V_0 is the initial volume, K is the carrying capacity, and α is the growth rate constant.

We qualitatively analyzed the evolution of the simulated variable z(t) (interpreted as tumor cell burden) and found that in the early months (months 1 to 4), the trajectory of z(t) closely resembles the Gompertzian sigmoid shape: initial exponential growth followed by a slowdown due to nonlinear damping effects. This behavior is expected for benign or slow-growing tumors.

However, as the control parameter ϱ and delay τ increase, the system undergoes bifurcations and enters chaotic regimes, diverging from the smooth Gompertz profile. This deviation is biologically plausible for aggressive tumors, where growth is influenced by stochastic mutations, angiogenesis bursts, and loss of regulatory feedback — all of which are captured dynamically by our delayed Lorenz-based model.

Therefore, the model not only reproduces classical tumor growth in early stages but also extends it by modeling the transition to complex, unstable, and chaotic dynamics seen in advanced cancer progression.

CONCLUSION

This work presented an innovative and mathematically robust approach to model cancer dynamics over 12 months, using a system of delayed differential equations (DDE) inspired by the Lorenz model, adapted to incorporate cellular memory effects such as proliferation, mutation and angiogenesis. The proposal breaks with traditional approaches by applying, in a pioneering way, advanced concepts of chaos theory, bifurcations and delayed dynamical systems in the simulation of tumor evolution, without considering immune system interventions or clinical treatments.

The progressive use of the delay parameter τ, month by month, allowed us to mathematically demonstrate how cancer can transition from an initial equilibrium state to a chaotic and disordered regime — behavior broadly compatible with what is observed in aggressive tumor environments in medical practice. The graphical representation by means of phase portraits (z(t)×y(t)) provided not only a clear visualization of the transition between stability, oscillation and chaos, but also served as a highly valuable instrument for understanding the intrinsic complexity of tumor cell growth.

Numerical simulations were performed using the Python language, using the fourth-order Runge-Kutta method to solve the delay differential equations. The algorithm was implemented to dynamically adjust the delay parameter τ every month of simulation, allowing precise analysis of the evolution of the system in different dynamic regimes. The NumPy library was used for vector calculations, while Matplotlib and SciPy assisted in graphical visualization and numerical integration.

The importance of this work for medicine is undeniable. Translating cell multiplication into precise mathematical language is an essential step towards a deep understanding of tumor progression. By quantifying cancer dynamics in numerical and structural terms, a new perspective is offered to predict critical states of the disease, as well as potential windows of intervention before the system reaches the point of no return. This type of modeling opens doors to the development of predictive and personalized strategies in oncological monitoring, contributing directly to precision medicine.

As a suggestion for future work, we highlight the possibility of including the immune system as a modulating agent of tumor dynamics, which would allow a simulation closer to clinical reality. In addition, new biological parameters can be incorporated into the model, such as the rate of cell necrosis, induced vascularization (quantitative angiogenesis) and response to chemotherapy. Expanding the model to multiscale systems or coupling it with artificial intelligence also represents a promising line of thought, aiming at the construction of predictive and personalized platforms for monitoring cancer at different stages.

REFERENCE

Binnewies, M., *et al.* (2018). Understanding the tumor immune microenvironment (TIME) for effective therapy. *Nature Medicine, 24*, 541–550. https://doi.org/10.1038/s41591-018-0014-x

Bray, F., *et al.* (2018). Global cancer statistics 2018: GLOBOCAN estimates of incidence and mortality worldwide for 36 cancers in 185 countries. *CA: A Cancer Journal for Clinicians, 68*(6), 394–424. https://doi.org/10.3322/caac.21492

Cardoso, R. P. (2021). Modelagem matemática aplicada ao crescimento de tumores. *Revista Brasileira de Biotecnologia e Cálculo Aplicado, 7*(2), 55–62

Chen, D. S., & Mellman, I. (2017). Elements of cancer immunity and the cancer–immune set point. *Nature, 541*(7637), 321–330. https://doi.org/10.1038/nature21349

Ferlay, J., *et al.* (2020). *Global Cancer Observatory: Cancer Today*. International Agency for Research on Cancer. https://gco.iarc.fr/today

Reis, L. M., & Almeida, F. C. (2020). Dinâmica de sistemas no estudo do câncer: Uma abordagem matemática. *Revista de Pesquisa Interdisciplinar em Ciências da Saúde, 12*(1), 88–95.

Seydel, R. (2010). *Practical bifurcation and stability analysis: From equilibrium to chaos* (2nd ed.). Springer.

Strogatz, S. H. (2018). *Nonlinear dynamics and chaos: With applications to physics, biology, chemistry, and engineering* (2nd ed.). CRC Press.

Lorenz, E. N. (1963). Deterministic nonperiodic flow. *Journal of the Atmospheric Sciences, 20*(2), 130–141. https://doi.org/10.1175/1520-0469(1963)020<0130:DNF>2.0.CO;2

Ruelle, D., & Takens, F. (1971). On the nature of turbulence. *Communications in Mathematical Physics, 20*(3), 167–192. https://doi.org/10.1007/BF01646553

Feigenbaum, M. J. (1978). Quantitative universality for a class of nonlinear transformations. *Journal of Statistical Physics, 19*(1), 25–52. https://doi.org/10.1007/BF01020332

May, R. M. (1976). Simple mathematical models with very complicated dynamics. *Nature, 261,* 459–467. https://doi.org/10.1038/261459a0

Packard, N. H., Crutchfield, J. P., Farmer, J. D., & Shaw, R. S. (1980). Geometry from a time series. *Physical Review Letters, 45*(9), 712–716. https://doi.org/10.1103/PhysRevLett.45.712